World Journal of Engineering Research and Technology
WJERT
www.wjert.org
SJIF Impact Factor: 7.029

SYNCHRONOUS STABILITY ANALYSIS OF PHASE-LOCKED SYSTEMS FOR MULTI-VOLTAGE SOURCE CONVERTERS BASED ON LYAPUNOV'S SECOND THEOREM

Qiuting Tan*

School of Science, Jiangxi University of Science and Technology, Ganzhou, 341000, China.

Article Received on 27/08/2024 **Article Revised on 17/09/2024** **Article Accepted on 07/10/2024**

***Corresponding Author**
Qiuting Tan
School of Science, Jiangxi University of Science and Technology, Ganzhou, 341000, China.

ABSTRACT

In the case of severe voltage plunge, the grid-connected voltage source converter (VSC) system based on phase-locked loop (PLL) synchronization is susceptible to transient instability and tripping from the grid. In this paper, the grid-connected systems of multi-paralleled VSCs are analyzed qualitatively by Lyapunov's second theorem method, and the corresponding stability criteria are constructed for the analysis of grid synchronous stability (GSS) of the multi-paralleled VSCs system. Firstly, the large signal model of the multi-paralleled VSCs system based on the PLL is constructed. Then, the GSS is quantitatively analyzed based on Lyapunov's second theorem method. At the same time, the influence of different working conditions (short-circuit ratio, voltage drop degree, and current injection amount) on the GSS of the multi-VSC system is revealed. Finally, the VSC-Infinite bus system is used as the test system to verify the accuracy of theoretical analysis in the Matlab/Simulink simulation platform. Theoretical analysis and simulation results show that the proposed method can provide reliable GSS evaluation.

KEYWORDS: Phase-locked loop, Multi-paralleled system, Lyapunov's second theorem method, Grid synchronous stability.

1. INTRODUCE

With the rapid development of power electronics technology and large-scale grid connection of renewable energy generation, a large number of renewable energy generating units

represented by photovoltaic and wind power are connected to the grid through VSC, which will lead to complex and profound changes in the synchronous stability mechanism of the power system.[1-3] Following the power system frequency through PLL is the key to achieving synchronization between VSC and the grid.[4-5] With the increasing penetration rate of renewable energy resources (RESs) in the system, the transient stability characteristics of the power system are increasingly dominated by PLL-based VSC.[6] When the system is subjected to large disturbances, such as power grid voltage drop, the nonlinear characteristics of PLL are the main cause of synchronous transient instability.[7-9] Therefore, it is urgent to analyze and evaluate the transient synchronization stability of the VSC under large disturbances. The synchronous dynamic process of PLL plays an important role in the transient stability of the VSC. PLL is essentially a nonlinear control system, and its nonlinear analysis is a challenging task.

At present, the PLL-based GSS problem has attracted extensive attention from academia and industry. From the perspective of the existence of an equilibrium point (EP), ref.[10] found that too deep a voltage drop or an inappropriate current reference value would cause the system to lose the EP, resulting in synchronous instability of VSC. However, refs.[11-13] shows that even if there is an EP, the system cannot guarantee a successful transition to a stable equilibrium point (SEP), and the GSS may still be lost due to poor dynamic processes, so the loss of synchronization (LOS) of VSC cannot be avoided. In addition, due to the mathematical similarity between PLL synchronization dynamics and the classical oscillation equations of synchronous generators (SG), SG's previous theory can help to understand the LOS of the VSC system. To describe the nonlinear behavior of PLL from a new physical perspective, the equal area criterion (EAC) method[14-17] can be introduced to reveal the synchronous instability mechanism, and it is found that LOS is essentially caused by the unbalanced input of PLL. Although these methods are heuristic in revealing the mechanisms of LOS, they are not suitable for rigorous GSS evaluation. Ref.[18] shows that the EAC method and the energy function method will lead to inaccurate estimation of the region of attraction (ROA) because the uncertain nonlinear damping effect must be ignored. The existence of indeterminate damping terms poses a great challenge to the application of direct methods. To solve this problem, ref.[19] considers the effect of infinite damping by defining the dissipative region, where the damping is positive, but the proposed method is more conservative. A new Lyapunov function (LF) is proposed in ref.[20], but it is not widely

applicable and effective in special cases. The study of large signal GSS for the grid-connected VSC mainly relies on calculation and simulation methods.

Due to the interpretability of the Lyapunov direct method, the direct method has been a promising development for decades. In[21], the second-order swing equation of the sagging control converter is constructed and the corresponding Lyapunov candidate function is derived. Ref.[22] simulated the external characteristics of SG and constructed the energy function based on the swing equation of VSG. It is worth mentioning that the above work takes a single-machine system as the research object, and the conclusion is not fully applicable to a multi-machine system. Inspired by the previous literature, this paper takes a multi-machine system as the research object, uses the Lyapunov direct method to deeply analyze and study the large signal GSS of grid-connected VSC, proposes a suitable LF and strictly formulates the analysis standard of GSS, and makes a credible GSS evaluation of the multi-machine system.

2. MODELING OF NONLINEAR DYNAMICAL SYSTEMS

2.1. System Description

The typical topology of parallel converters in grid-connected RES systems is shown in Figure 1. Large wind farms consisting of the multi-parallel VSC system pass through their respective line impedance $Z_k(k=1,\ldots,N)$ aggregation to the point of common coupling (PCC) and are subsequently integrated into the grid via a public transmission line. The grid is modeled as an equivalent impedance Z_g in series with an ideal voltage source U_g. In addition, $L_{f,k}, C_{f,k}$ represents the filter inductance and filter capacitance respectively. VSC uses voltage-directed current control, where synchronous reference frame-based PLL is commonly used for synchronization. PLL adjusts angular velocity and provides a synchronization phase by detecting the voltage at PCC points. In general, since the bandwidth of the PLL is much smaller than the bandwidth of the current loop, and the current loop can be assumed to be ideal in the time scale of the PLL (i.e., $I_d = I_d^*, I_q = I_q^*$).[23]

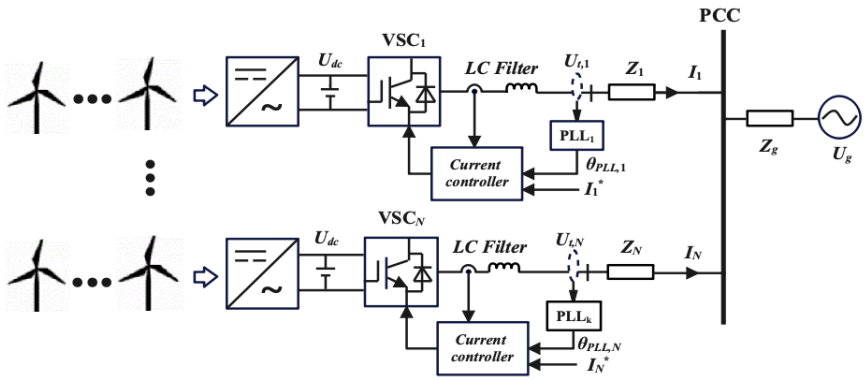

Fig. 1: Typical topology of parallel converters in grid-connected RES systems.

2.2. Nonlinear system modeling

Based on the typical VSC structure topology shown in FIG. 1, the voltage vector $U_{tq,i}$ of the terminal voltage of the *i-th* VSC can be given by equation (1) according to Kirchhoff's voltage/current law and the current reference direction.

$$U_{t,i} = U_g e^{j\theta_g} + Z_i I_i^* + Z_g \sum_{j=1, j\neq i}^{N} I_j^* e^{j(\theta_{Zg}+\theta_{ij})} \qquad (1)$$

Fig. 2(a) shows the PLL control block diagram. In the multi-VSCs system, the grid model is usually established based on the rotating coordinate system as shown in Fig. 2(b), and the *DQ* coordinate system is defined as a common frame, taking the phase angle θ_g of time-varying grid voltage U_g as the reference vector.

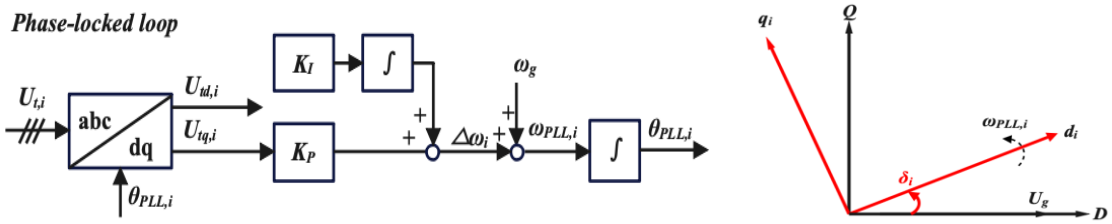

(a) **(b)**

Fig. 2: (a) PLL control block diagram; (b) Public *DQ*-frames of the system and local *dq*-frames of VSC$_k$.

In local *dq*-frames, $U_{tq,i}$ is the input to the proportional integration (PI) controller of the PLLi. Therefore, the equation of state for PLLk can be given by equation (2).

$$\begin{cases} \dfrac{d\delta_i}{dt} = \Delta\omega_i \\ \dfrac{d\Delta\omega_i}{dt} = K_P \dfrac{dU_{tq,i}}{dt} + K_I U_{tq,i} \end{cases} \qquad (2)$$

Where, the power angle $\delta_i = \theta_{PLL,i} - \theta_g$ represents the angle difference between $U_{t,i}$ and U_g, $\Delta\omega_i = \omega_i - \omega_0$ represents the angular velocity difference between PLL_i and U_g, and K_P and K_I are the proportional gain and integral gain of PLL_k, respectively.

Based on the principle of coordinate transformation, the *q*-axis component of the terminal voltage $U_{t,i}$ can be given by the following formula,

$$U_{tq,i} = -U_g \sin\delta_i + X_g I_{d,i}^* + R_g I_{q,i}^* + \sum_{j=1, j\neq i}^{N} Z_g I_j^* \sin\left(\theta_{Zg} + \theta_j - \delta_{ij}\right) \qquad (3)$$

Where $\delta_{ij} = \delta_i - \delta_j$, in simultaneous equations (2) and (3), the large signal model of a multi-parallel VSC system can be derived as an oscillation equation similar to SG, aås shown in equation (4).

$$J_i \frac{d^2\delta_i}{dt^2} = P_{m,i} - U_g \sin\delta_i - (\gamma_i - D_i \cos\delta_i)\Delta\omega_i \qquad (4)$$

Where, J_i, $P_{m,i}$ and $(\gamma_i - D_i \cos\delta_i)$ represent the virtual inertia, the virtual input mechanical power, and the virtual damping effect respectively. The detailed mathematical expression is summarized as follows,

$$\begin{cases} J_i = \dfrac{1 - K_p(L_i + L_g)I_{d,i}^*}{K_i} \\ P_{m,i} = X_g I_{d,i}^* + R_g I_{q,i}^* + \sum\limits_{j=1, j\neq i}^{N} Z_g I_j^* \sin\left(\theta_{Zg} + \theta_j - \delta_{ij}\right) \\ \gamma_i = (L_i + L_g)I_{d,i}^* \\ D_i = \dfrac{K_p}{K_i} U_g \end{cases} \qquad (5)$$

3. TRANSIENT SYNCHRONIZATION STABILITY ANALYSIS

3.1. Construction of the Lyapunov function

In this section, the Lyapunov candidate function of VSC is derived from the first integral method.[24] In general, ignoring the damping effect, the Lyapunov candidate function can be expressed as,

$$V(\delta, \Delta\omega) = \sum_{i=1}^{N} \underbrace{J_i \int_0^{\Delta\omega_i} \dot{\omega}_i \Delta d\Delta\omega_i}_{V_k:\text{Kinetic energy}} - \underbrace{\int_{\delta_{s,i}}^{\delta_i} \left(P_{m,i}\delta_i + U_g \sin\delta_i\right) d\delta_i}_{V_p:\text{Potential energy}} \qquad (6)$$

Where, $\delta_{s,k}$ is SEP of VSC_k. Through integral calculation, equation (6) can be further written as,

$$V(\delta,\Delta\omega)=\sum_{i=1}^{N}\left(\frac{1}{2}J_i\Delta\omega_i^2-P_{m,i}\delta_i-V_g\cos\delta_i+V_0\right) \quad (7)$$

Where, the constant $V_0=P_{m,i}\delta_{s,i}-U_g\cos\delta_{s,i}$. The derivative of $V(\delta,\Delta\omega)$ is given by equation (8).

$$\frac{dV(\delta,\Delta\omega)}{dt}=-\sum_{i=1}^{N}D_{eq,i}\Delta\omega_i^2 \quad (8)$$

Make a physical interpretation of the LF given by equation (7) and check whether the candidate function meets all the criteria to be a suitable LF. To verify suitability, first check whether the candidate function is positive definite in the neighborhood and whether there is SEP such that $V(\delta_s,0)=0$. Finally, the negative qualitative or negative semi-qualitative of the derivative (8) is verified. Detailed verification is as follows:

(1) According to the steady-state equation of the VSC system, $V(\delta_s,0)=0$.

(2) The kinetic energy $V_k=\sum_{i=1}^{N}\frac{1}{2}J_i\Delta\omega_i^2$ is globally positive definite; Fig. 3 shows the curve of equivalent potential energy V_p. At SEP$(\delta=\delta_s,\Delta\omega=0)$, V_p is greater than 0 and $\delta_s\in(0,\pi/2)$ is the local minimum of V_p; Within the feasible working range $\delta\in(-\pi-\delta_s,\pi-\delta_s)$ of the grid-connected converter, $V_p>0$. It can be shown that there is a neighborhood within the neighborhood of δ_s, and SEP exists such that $V_k(\delta_s,0)=0$ and $V_k(\delta,\Delta\omega)$ are positive definite.

(3) When condition $D_i\geq 0$ is satisfied, it can be obtained that $\frac{dV(\delta,\Delta\omega)}{dt}$ is negative qualitative in the range of $\delta_i\in\left(-\arccos\frac{D_i}{\gamma_i},\arccos\frac{D_i}{\gamma_i}\right)$.

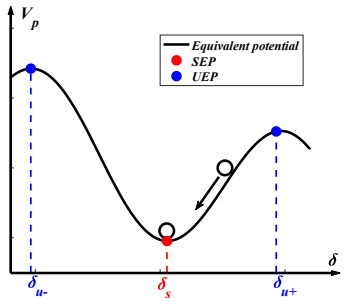

Fig. 3: Curve of equivalent potential energy V_p. At UEP, V_p reaches a local maximum. At SEP, V_p reaches a local minimum.

Therefore, the proposed Lyapunov function (Prop.LF) by equation (7) is a suitable candidate function for GSS analysis of multi-VSC systems.

3.2 Analytical criteria of GSS

Generally, without considering the nonlinear damping effect, the critical transient energy V_{cr} of a multi-parallel VSC grid-connected system can be obtained at the unstable equilibrium point UEP. The expression of V_{cr} is as follows.

$$V_{cr} = V\left(\delta, \Delta\omega\right) = \sum_{i=1}^{N} V_k\left(\delta_{u,i}, \Delta\omega_{u,i}\right) \qquad (9)$$

As long as the following inequality (10) is satisfied, the GSS of the system can be maintained during the failure.

$$V(\delta, \Delta\omega) < V_{cr} \qquad (10)$$

The analytical GSS index can be defined as follows,

$$\lambda_{GSS} = V(\delta, \Delta\omega) - V_{cr} \qquad (11)$$

When $\lambda_{GSS} > 0$, it means that the system is in a stable state, and the larger s is, the higher the stability margin of the system VSC_k is, that is, the better the GSS is. Stability index λ_{GSS} provides an efficient and practical method for checking whether VSCs reach the GSS state. Importantly, λ_{GSS} can be determined without solving nonlinear differential equations, which provides a convenient and efficient method for the GSS of systems. Using Lyapunov's second theorem method to analyze the transient castability of multiple VSC-infinite bus systems, the steps are as follows:

(1) Calculate steady-state power flow.

(2) Determine the critical energy value.

(3) The transient synchronous stability criteria are as follows:

(a) $\lambda_{GSS} > 0$, the system is in a stable state;

(b) $\lambda_{GSS} = 0$, the system is in transient critical stability;

(c) $\lambda_{GSS} < 0$, the system is in a transient instability.

4. SIMULATION VERIFICATION

Four parallel VSC nonlinear models as shown in Fig. 4 were selected for the experiment. First, Lyapunov's second theorem is used to describe the synchronous stability domain of

multiple parallel VSC grid-connected systems, and then the time-domain simulation is carried out on the simulation platform of Matlab/Simulink to verify the correctness of the proposed GSS criterion. Parameters of the test system are shown in Table I, simulating an LOS event. At t = 0.5s, the infinite bus voltage drops to 0.2 *p.u.*

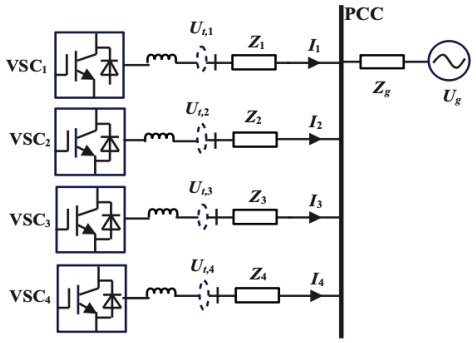

Fig. 4: Multi-VSC-infinite bus system.

Table I: System Parameters.

Symbols	Description	Value
K_P/K_I	PI parameters of PLL	0.30/20
$Z_1(R_1/X_1)$	Line impedance of VSC_1	0.019+j0.065 *p.u.*
$Z_2(R_2/X_2)$	Line impedance of VSC_2	0.017+j0.055 *p.u.*
$Z_3(R_3/X_3)$	Line impedance of VSC_3	0.015+j0.045 *p.u.*
$Z_4(R_4/X_4)$	Line impedance of VSC_4	0.013+j0.035 *p.u.*
$Z_g(R_g/X_g)$	Grid impedance	0.12+j0.326 *p.u.*
$I_{d,i}^*$	Reference active current injection	0.23/0.22/0.21/0.20 *p.u.*
$I_{q,i}^*$	Reference reactive current injection	-0.10/-0.08/-0.06/-0.04 *p.u.*

4.1. Synchronous stability region estimation based on LF

To quantify the effect of system parameters on the transient stability boundary, the ROA of SEP is adopted in this section. At a fixed level, ROA is estimated by generating a contour plot of the Lyapunov function provided by equation (18). The concept of ROA is further extended to estimate the critical clearance time (CCT) of multiple parallel VSC grid-connected systems under grid faults. CCT is estimated by the fault trajectory of the grid-connected system, that is, the intersection of the LF fault trajectory and point. Fig. 4(a) shows the CCT results estimated by Prop. LF. It can be found that when t=0.5s, the grid voltage plummets, and the CCT is 0.46s from the moment the fault starts. Fig. 4(b) shows the results of transient stability boundary estimation by Prop. LF. When the fault clearing time is $t \le t_{cr}$ and the fault path is within ROA, the system can maintain GSS. If a fault ($t > t_{cr}$) is not removed in time, the fault trajectory will leave ROA, and LOS events will inevitably occur. It

can be seen from the above simulation results that the equivalent energy surface solved by Lyapunov's second theorem can effectively evaluate the transient synchronous stability region of the system, which is of great significance for the analysis of GSS of multi-parallel VSCs system.

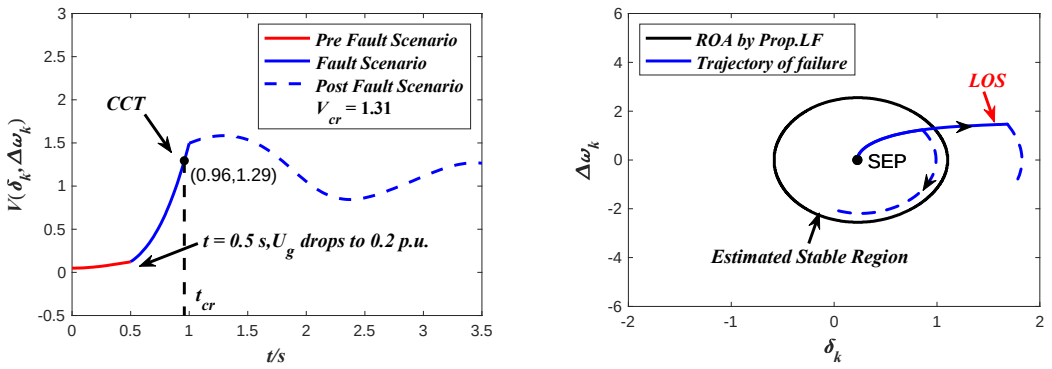

(a) **(b)**

Fig. 5: (a)CCT calculation; (b) ROA estimation and fault trajectory based on Prop.LF.

4.2 Synchronous stability region validation

Case 1: The GSS of a multi-parallel VSC grid-connected system with different short-circuit ratios SCR (1.5, 2,2.6, respectively) was evaluated using Prop. LF. According to the approximate estimation of ROA shown in Fig. 6, it is not difficult to find that the ROA of the equilibrium point shrinks as the system strength defined by SCR decreases. On the other hand, the estimated ROA swells as the PLL bandwidth decreases. These theoretical results prove that the transient stability boundary of nonlinear systems increases with the increase of system strength.

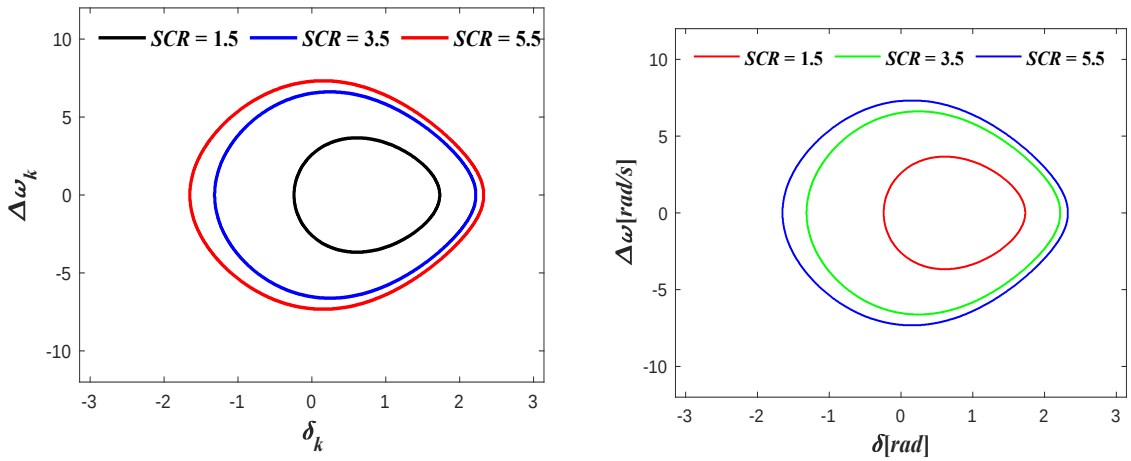

Fig. 6: ROA estimation under different SCR parameters.

To verify the above conclusions, three groups of cases (*SCR*=1.5, 2, and 2.6) were simulated in the time domain on the Simulink platform. Fig. 7(a) and (b) show the simulation results of the PLL phase angle θ_{PLL} and VSC terminal voltage U_t respectively. It can be found that when SCR decreases continuously, the amplitude of θ_{PLL} and U_t amplitude oscillations increases. When *SCR*=1.5, θ_{PLL} has an irreversible continuous oscillation, and U_t also has a continuous oscillation, which cannot be stabilized. At this time, the system loses synchronization with the power grid, and the system loses stability.

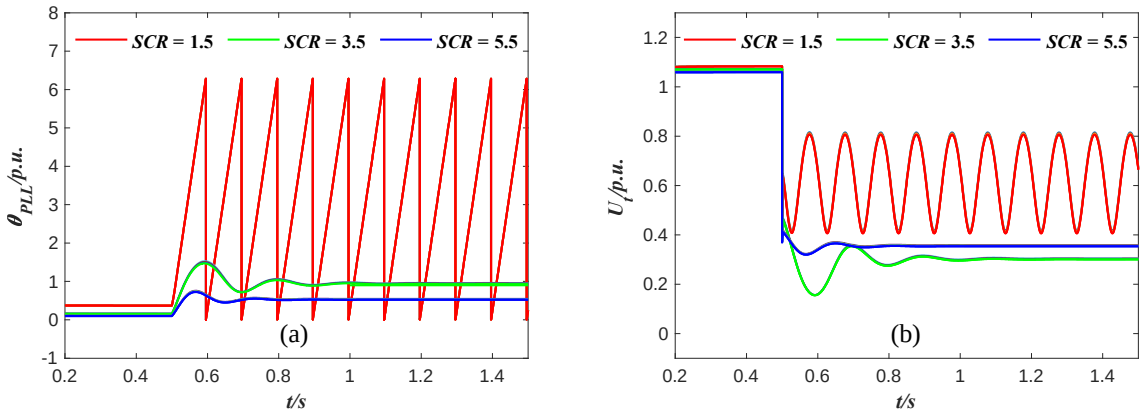

Fig. 7: Time domain simulation. (a) Phase Angle of PLL θ_{PLL}; (b) Terminal voltage U_t of VSC.

Case 2: As shown in Fig. 8, Prop.LF was used to evaluate the GSS of the multi-parallel VSC systems with different grid voltage U_g drops to (0.15 *p.u*, 0.3 *p.u*, 0.5 *p.u*.). It can be found from the results that ROA gradually decreases with the intensification of voltage drop, resulting in the weakening of GSS and the increased risk of LOS occurrence.

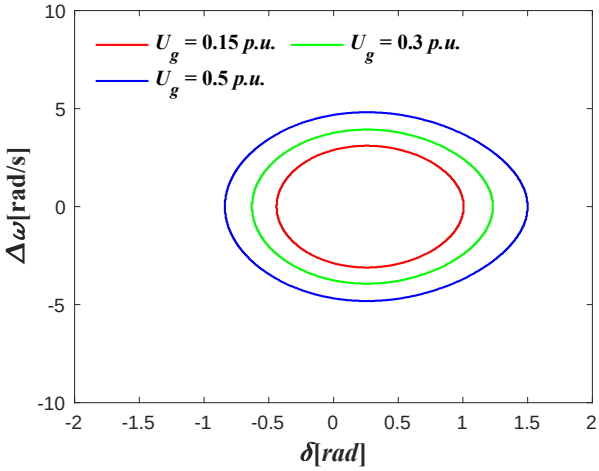

Fig. 8: ROA estimation under U_g sag parameters of different grid voltages.

To verify the above conclusions, three groups of cases (U_g=0.15 *p.u*, 0.3 *p.u*, and 0.5 *p.u*.) for time domain simulation. The corresponding simulation results are shown in Fig. 9. When the U_g drop degree intensifies, the amplitude of θPLL oscillation increases, and even irreversible continuous oscillation occurs, while Ut also occurs continuous oscillation. When U_g drops to 0.5, LOS events occur, and the deeper the U_g drop is, the more detrimental it is for wind power systems to maintain GSS.

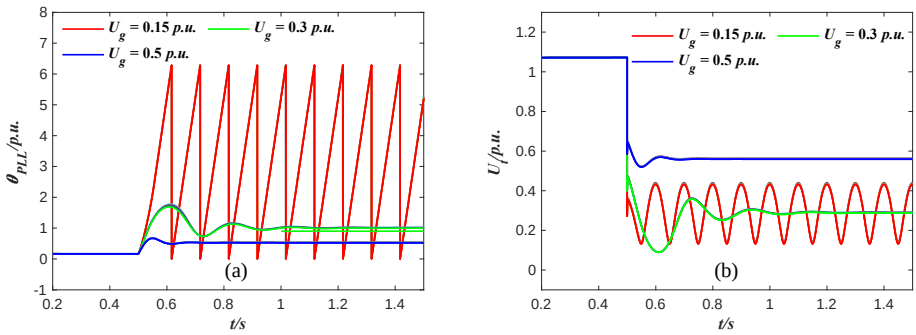

Fig. 9: Time domain simulation. (a) Phase Angle of PLL θ_{PLL}; (b) Terminal voltage U_t of VSC.

Case 3: Fig. 10 shows the effect of different VSC current injection amounts on ROA. Observe the results of Fig. 10(a), reactive current injection ($I_q^* < 0$) is fixed, and ROA decreases with the increase of active current injection (I_d^*). Therefore, increasing the D-axis current of the wind farm weakens the GSS of the system. Similarly, as shown in Fig. 10(b), when I_d^* is fixed, ROA increases as I_q^* increases. This indicates that reasonable increase of I_q^* can improve the GSS of the system during failure. Therefore, the current injection amount of the VSC should be correctly set according to the analytical GSS standard to maintain the GSS of the system.

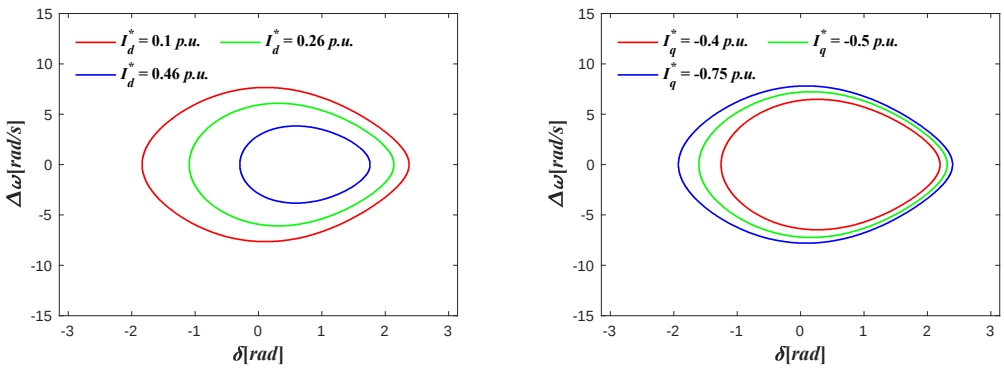

Fig. 10: ROA estimation under different current injection quantities.

Next, for active current injection (0.1 *p.u*, 0.26 *p.u*, and 0.46 *p.u*.) and reactive current injection (-0.4 *p.u*, -0.50 *p.u* and -0.75 *p.u*.) case for time domain simulation. Fig. 11 shows the simulation results of I_d^* under different conditions. It can be found that increasing the injection amount of I_d^* will cause the oscillation amplitude of θ_{PLL} and U_t to increase, thus weakening the GSS of the VSC system and increasing the risk of LOS. When I_d^* increases to 0.26 and 0.46, PLL is out of sync with the grid and LOS cannot be avoided. Fig. 12 shows the simulation results under different I_q^* conditions. It can be found that increasing the injection amount of I_q^* will cause the oscillation amplitude of θ_{PLL} and U_t to decrease, which is beneficial to the GSS of the system. When I_q^* is set to -0.4, the PLL is out of sync with the grid and the wind system cannot maintain GSS.

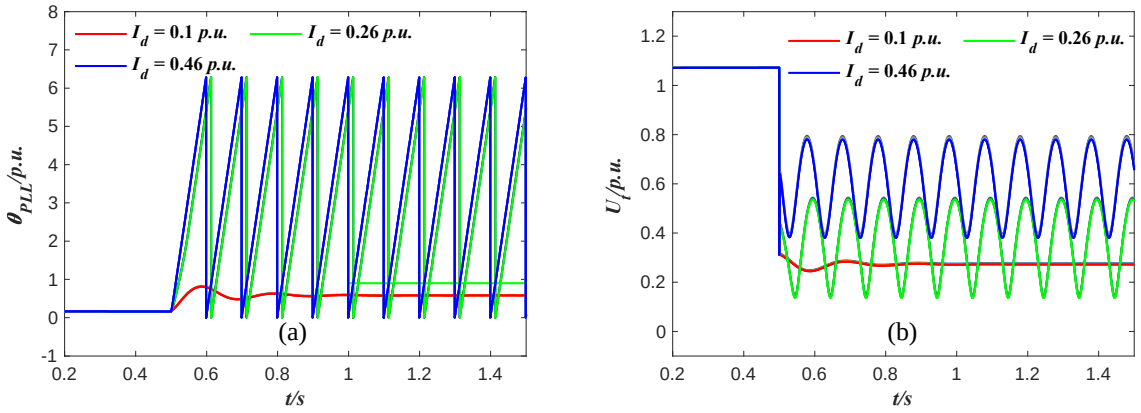

Fig. 11: Time domain simulation. (a) Phase Angle of PLL θ_{PLL}; (b) Terminal voltage U_t of VSC.

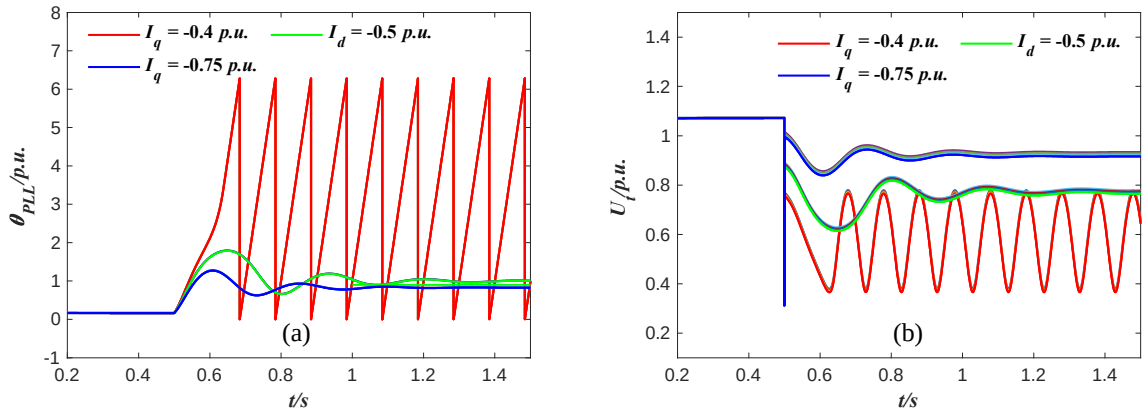

Fig. 12: Time domain simulation. (a) Phase Angle of PLL θ_{PLL}; (b) Terminal voltage U_t of VSC.

5. CONCLUSION

In this paper, based on Lyapunov's second theorem, the sufficient stability criterion for direct analysis of transient synchronous stability of multi-parallel VSCs system is derived in a generalized way. The rigorously constructed GSS criterion is applied to the quantitative analysis of GSS for multi-parallel VSCs system. GSS criteria provide an efficient and practical method for checking whether VSCs have reached GSS status. Importantly, GSS criteria can be determined without solving nonlinear differential equations, which provides a convenient and effective method for quantitative analysis of GSS. In addition, under different working conditions (short-circuit ratio, voltage drop degree, and current injection amount), the GSS of the multi-parallel VSCs system is quantitatively studied. Based on the GSS criterion, the transient synchronous stability domain boundary of the multi-parallel VSCs system can be obtained. Based on the estimation results of transient synchronous stability region boundary under different short-circuit ratios, grid voltage drop degrees, and current injection quantity, it can be found that large short-circuit ratio, small grid voltage fault degree, small active current injection, and large reactive current injection are conducive to GSS of multi-machine system. Finally, the VSC-Infinite bus system is used as the test system, and the accuracy of the theoretical analysis is verified by Simulink simulation. Theoretical analysis and simulation results show that the proposed method can provide reliable GSS evaluation.

6. REFERENCE

1. Zha X, Huang M, Liu Y, Tian Z. An overview on safe operation of grid-connected converters from resilience perspective: Analysis and design. Int J Electr Power Energy Syst, December, 2022; 143: 108511.
2. Shang L, Hu J, Yuan X, Huang Y. Improved virtual synchronous control for grid connected VSCs under grid voltage unbalanced conditions. J. Mod. Power Syst. Cle., 2019; 7(1): 174–85.
3. Zhou P, et al. Stability of DC-link voltage as affected by phase locked loop in VSC when attached to weak grid. In: 2014 IEEE PES General Meeting | Conference & Exposition, 2014; 1–5.
4. X. Wang and F. Blaabjerg, “Harmonic stability in power electronic based power systems: Concept, modeling, and analysis,” IEEE Trans. Smart Grid, May 2019; 10(3): 2858–2870.

5. M. G. Taul, X. Wang, P. Davari, and F. Blaabjerg, “Reduced-order and aggregated modeling of large-signal synchronization stability for multi-converter systems,” IEEE J. Emerg. Sel. Topics Power Electron., Jun. 2021; 9(3): 3150–3165.
6. Abdelrahem M, Hackl CM, Kennel R. Finite position let-phase locked loop for sensorless control of direct-driven permanent-magnet synchronous generators. IEEE Trans. Power Electron, 2018; 33(4): 3097–105.
7. M.G. Taul, X. Wang, P. Davari, F. Blaabjerg, Reduced-order and aggregated modeling of large-signal synchronization stability for multiconverter systems, IEEE J. Emerg. Sel. Top. Power Electron, 2021; 9(3): 3150–3165.
8. J. Pei, J. Yao, R. Liu, D. Zeng, P. Sun, H. Zhang, Y. Liu, Characteristic analysis and risk assessment for voltage-frequency coupled transient instability of large-scale grid-connected renewable energy plants during LVRT, IEEE Trans. Ind. Electron, Jul. 2020; 67(7): 5515–5530.
9. C. Zhang, et al., Modeling and analysis of grid-synchronizing stability of a Type-IV wind turbine under grid faults, Int. J. Electr. Power Energy Syst, 2019; 117.
10. Goksu ¨ O, ¨ Teodorescu R, Bak CL, Iov F, Kjær PC. Instability of wind turbine converters during current injection to low voltage grid faults and PLL frequency based stability solution. IEEE Trans Power Sys., July. 2014; 29(4): 1683–91.
11. Liu Y, Yao J, Pei J, Zhao Y, Chen S. Transient Stability Enhancement Control Strategy Based on Improved PLL for Grid-Connected VSC during Severe Grid Fault. IEEE Trans Energy Convers, Mar., 2021; 36(1): 218–29.
12. He X, Geng H, Li R, Pal BC. Transient stability analysis and enhancement of renewable energy conversion system during LVRT. IEEE Trans Sustain Energy, Jul., 2020; 11(3): 1612–23.
13. Zhang Y, Zhang C, Cai X. Large-Signal Grid-Synchronization Stability Analysis of PLL-Based VSCs Using Lyapunov’s Direct Method. IEEE Trans Power Sys, Jan., 2022; 37(1): 788–91.
14. C. Zhang, X. Cai, A. Rygg and M. Molinas, "Modeling and analysis of grid-synchronizing stability of a Type-IV wind turbine under grid faults", Int. J. Elect. Power Energy Syst., 2020; 117: 105544-105544.
15. Hu Qi, Fu L, Ma F, Ji F. Large signal synchronizing instability of PLL-based VSC connected to weak AC grid. IEEE Trans. Power Syst., 2019; 34(4): 3220–9.
16. He X, Geng H, Ma S. Transient stability analysis of grid-tied converters considering PLL’s nonlinearity. CPSS Trans. Power Elec. Appl., 2019; 4(1): 40–9.

17. Zhang C, Cai Xu, Rygg A, Molinas M. Modeling and analysis of grid-synchronizing stability of a type-IV wind turbine under grid faults. Int. J. Elect. Power, 2020; 117: 105544.
18. Y. Zhang, C. Zhang and X. Cai, "Large-Signal Grid-Synchronization Stability Analysis of PLL-Based VSCs Using Lyapunov's Direct Method," in IEEE Transactions on Power Systems, Jan. 2022; 37(1): 788-791.
19. M. Z. Mansour, S. P. Me, S. Hadavi, B. Badrazadeh, A. Karimi and B. Bahrani, "Nonlinear transient stability analysis of phased-locked loop based grid-following voltage source converters using Lyapunov's direct method", IEEE J. Emerg. Sel. Top. Power Electron.
20. S. Ma, H. Geng, L. Liu, G. Yang and B. C. Pal, "Grid-synchronization stability improvement of large scale wind farm during severe grid fault", IEEE Trans. Power Syst., Jan. 2018; 33(1): 216-226.
21. Kabalan M, Singh P, Niebur D. Nonlinear Lyapunov stability analysis of seven models of a DC/AC droop controlled inverter connected to an infinite bus. IEEE Trans. Smart Grid, 2019; 10(1): 772–81.
22. Shuai Z, Shen C, Liu X, Li Z, Shen ZJ. Transient angle stability of virtual synchronous generators using Lyapunov's direct method. IEEE Trans. Smart Grid., 2019; 10(4): 4648–61.
23. S.-K. Chung, "A phase tracking system for three phase utility interface inverters," IEEE Trans. Power Electron., May 2000; 15(3): 431–438.
24. M. Zarif Mansour, et al. "Nonlinear Transient Stability Analysis of Phased-Locked Loop-Based Grid-Following Voltage-Source Converters Using Lyapunov's Direct Method," in IEEE Journal of Emerging and Selected Topics in Power Electronics, Jun. 2022; 10(3): 2699-2709.